Kidney Diseases

Research Article

Kidney Dis 2022;8:308–318
DOI: 10.1159/000524164

Received: February 9, 2022
Accepted: March 17, 2022
Published online: May 30, 2022

Treatment of Membranous Nephropathy by Disulfiram through Inhibition of Podocyte Pyroptosis

Daoyuan Lv[a, b] Song Jiang[b] Mingchao Zhang[b] Xiaodong Zhu[b] Fan Yang[b] Hui Wang[b] Shen Li[b] Feng Liu[b] Caihong Zeng[b] Weisong Qin[b] Limin Li[c] Zhihong Liu[a, b]

[a]Department of Nephrology, Jinling Hospital, The First School of Clinical Medicine, Southern Medical University, Nanjing, China; [b]National Clinical Research Center of Kidney Diseases, Jinling Hospital, Nanjing, China; [c]School of Life Science and Technology, China Pharmaceutical University, Nanjing, China

Keywords
Membranous nephropathy · Disulfiram · Pyroptosis · Podocyte

Abstract
Introduction: Membranous nephropathy (MN) is a common chronic kidney disease in adults and a major challenge of clinical practice for its treatment. Despite major advances, since the discovery of the phospholipase A2 receptor as the major autoantigen of podocytes in MN, the mechanisms leading to glomerular damage remain elusive. Pyroptosis, a newly discovered type of programed necrotic cell death mainly mediated by gasdermin, was found to be responsible for podocyte injury in MN in our recent work. ***Objectives:*** The aim of this study was to explore the therapeutic effect of an FDA-approved drug, disulfiram (DSF), in the treatment of MN by inhibiting pyroptosis. ***Methods and Results:*** DSF significantly alleviated C3a/C5a-induced podocyte injury in vitro and renal lesions in passive Heymann nephritis (PHN) rats, as reflected by the decreased percentage of propidium iodide staining podocytes, decreased lactate dehydrogenase release from cultured podocytes and improvement in 24-h urine protein, serum albumin, serum creatinine, abnormal alterations of podocyte injury markers Desmin and WT-1 and podocyte foot process fusion in PHN rats. The protective effect of DSF on podocyte injury in vitro and in vivo can be ascribed to its inhibition of the activation and membrane translocation of the pyroptosis executor gasdermin D (GSDMD) in podocytes. DSF also inhibited the increase and activation of the pyroptosis signaling pathway NLRP3-ASC-Caspase-1/IL-18/GSDMD in C3a/C5a-treated podocytes and renal tissue of PHN rats. ***Conclusion:*** DSF is a potential drug for MN treatment, and its clinical application needs to be further investigated.

Introduction

Membranous nephropathy (MN) is one of the most common causes of chronic kidney disease in adults and one of the leading causes of end-stage renal disease [1]. In recent years, the morbidity of MN has increased rapidly in China as well as in other developing countries, imposing a great burden on the medical system and social economy [2–4]. MN is characterized by an accumulation of immune deposits on the subepithelial aspect of the glo-

Karger@karger.com
www.karger.com/kdd

Correspondence to:
Limin Li, liminli@cpu.edu.cn
Zhihong Liu, liuzhihong@nju.edu.cn

merular capillary wall by the podocyte. Antibodies that target podocyte or planted antigens accumulate as immune deposits, resulting in activation of the complement system, thus generating the complement-active fragments and finally leading to injury of the podocyte and filtration barrier. Although planted antigens such as cationic BSA or autoantigens of podocytes, including phospholipase A2 receptor, thrombospondin type-1 domain-containing 7A, exostosin 1/2 complex, neural epidermal growth factor-like 1, semaphorin 3B and protocadherin 7, have been found and the underlying mechanisms of complement-induced podocyte injury in MN, including oxidative stress, endoplasmic reticulum stress, apoptosis, alterations of the cytoskeleton and slit diaphragm, have been illustrated [5–7], the panorama of the process of podocyte damage is far from complete. To date, treatment of MN has focused on nonspecific immunosuppressive therapy, similar to most other autoimmune diseases, and a major dilemma of current treatment is efficacy versus toxicity, especially prevention of MN progression. Therefore, understanding the mechanisms of podocyte injury in MN and exploring more effective targeted drugs may pave the way for better therapy for MN patients.

Pyroptosis is gasdermin-mediated programed necrotic cell death. It features cell swelling and eventual lysis caused by gasdermin pore formation in the plasma membrane. The oligomerization of the gasdermin-N domain of gasdermin D (GSDMD) after cleavage of GSDMD by canonical inflammasomes activation is a pivotal pathway that drives pyroptosis [8]. Canonical inflammasomes are multimeric complexes that consist of a nucleotide-binding oligomerization domain-like receptor (NLR) or absent in melanoma 2-like receptor pattern recognition receptor, apoptosis-associated speck-like protein containing a CARD (ASC) and Caspase-1 [9]. Once activated, canonical inflammasomes activate Caspase-1, leading to cleavage of GSDMD and maturation of IL-1β and IL-18, conferring a highly pro-inflammatory phenotype that is different from that of other types of necrosis [10]. Recently, our group first depicted the involvement of pyroptosis, driven by the activation of the canonical inflammasome NLRP3, in the pathogenesis of podocyte injury in MN [11]. Understanding the molecular mechanisms of pyroptosis-mediated podocyte injury in MN not only reveals the pathogenesis of this disease but may also help to develop novel treatments.

The FDA-approved drug tetraethylthiuram disulfide (disulfiram, DSF) is a potent inhibitor of aldehyde dehydrogenase that is responsible for the conversion of alcohol into acetaldehyde and has long been used for alcohol addiction in clinical practice since the 1950s [12]. Recently, DSF was found to inhibit GSDMD pore formation by modifying a conserved cysteine in GSDMD and therefore has an anti-pyroptotic effect [13]. We are interested in this finding and wonder whether the pyroptosis inhibitor DSF has a therapeutic effect on MN by alleviating podocyte injury. In this study, we evaluated the effect and mechanisms of the pyroptosis inhibitor DSF on podocyte injury in MN in vitro and in vivo by using a complement-induced podocyte damage model and the passive Heymann nephritis (PHN) rat model, respectively, to illustrate the therapeutic effect of DSF on MN.

Materials and Methods

Cell Culture and Treatments

A conditionally immortalized human podocyte cell line was kindly provided by Dr. Saleem (University of Bristol, Bristol, UK). The cells were cultured as previously described [14]. Podocytes were treated with 50 nM C3a or C5a for 1 h to establish a complement-induced podocyte damage model. The dosage effect of DSF at gradient concentrations between 50 nM and 1 μM on podocyte protection was explored according to lactate dehydrogenase (LDH) release in our preliminary experiment and 250 nM, the optimal dose, was added 1 h prior to model establishment for further investigation.

Propidium Iodide Staining

Cultured podocytes were stained with propidium iodide (PI) (3.34 μg/mL) at 37°C for 20 min and then incubated with DAPI (15 μg/mL) at 37°C for 20 min for nuclear staining. Photomicrographs were captured with confocal microscopy (LSM710; Carl Zeiss Meditec AG, Oberkochen, Germany).

LDH Release Assay

LDH release from cultured podocytes in the supernatant was detected using an LDH Cytotoxicity Assay Kit (Beyotime Biotechnology, Shanghai, China) according to the manufacturer's instructions. Briefly, LDH was assessed based on the chromogenic reaction of 2-p-iodophenyl-3-nitrophenyl tetrazolium chloride catalyzed by diaphorase, and LDH levels were semiquantified via a colorimetric method.

Induction of PHN

Rabbit anti-Fx1A serum was prepared according to Dr. Salant's protocols and concentrations of anti-Fx1A antibody in the serum were measured by immunofluorescence staining of rat proximal renal tubular epithelial cell brush border [15]. Female SD rats weighing 150–180 g were obtained from Sino-British SIPPR/BK Lab (Shanghai, China). All rats were housed under standard conditions and provided rat chow and water ad libitum in the Experimental Animal Center of Jinling Hospital. Protocols for the animal studies were approved by the Institutional Animal Care and Use Committee of Jinling Hospital, the First School of Clinical Medicine of Southern Medical University, Nanjing, China (Approval

reference number: 2019JLHGKJDWLS-136). Rats were intraperitoneally injected with 2- and 1-mL anti-Fx1A antiserum at 1 h intervals to establish the PHN model. For the normal control group (NC), rats were injected with normal rabbit serum in the same amount at the same intervals.

Drug Treatment of PHN Rats

DSF was obtained from Aladdin Co., Ltd. (Shanghai, China). DSF was suspended in 0.5% sodium carboxymethyl cellulose and administered at a dosage of 50 mg/kg to PHN rats via gavage, bid; intervention was given 1 day prior to Fx1A antiserum injection and maintained throughout the observation period. Rats that died accidentally or had 24 h urine protein (24 h-UPro) <10 mg on the 8th day after model establishment were discarded. Finally, 6 rats from each group were included for further analysis.

Urine Protein and Blood Biochemistry Test

The 24 h-UPro of rats was tested using the Bradford method. The serum of rats was separated from fresh blood for blood biochemistry tests, including serum creatinine (SCr), blood urea nitrogen (BUN), albumin (ALB), total cholesterol (T-CHOL), triglyceride (TG), high-density lipoprotein (HDL) and low-density lipoprotein (LDL), using an automatic biochemical analyzer (7180 automatic analyzer; Hitachi, Ltd., Tokyo, Japan).

Histopathology

Renal tissues were fixed with 10% formaldehyde for more than 6 h and then infiltrated with and embedded in paraffin after dehydration and clearing. After deparaffination and rehydration, the 2.5-μm thick sections were separately stained with Masson trichrome staining and periodic acid silver methenamine (PASM)-Masson staining. Photomicrographs of the sections were obtained with a light microscope (Eclipse 80i; Nikon Instruments Inc., Tokyo, Japan).

Transmission Electron Microscopy

For each animal, approximately 1 mm^3 of renal tissue was fixed with 2.5% glutaraldehyde at 4°C for more than 4 h. Tissues were subsequently washed with PBS for 3 times and postfixed with 1% osmium tetroxide at room temperature (RT) for 1 h. Ultrathin sections (70-nm thick) were stained with uranyl acetate and lead citrate. After drying, the stained specimens were observed, and photomicrographs were acquired with an electron microscope (H-7500; Hitachi, Ltd., Tokyo, Japan). The average foot process width of podocytes was calculated according to formula: $(\pi/4) \times (\Sigma$ glomerular basement membrane (GBM) length/Σ number of foot process) by using DigitalMicrograph software (Gatan, Inc., Pleasanton, CA, USA) as previously described [16].

Immunofluorescence

For cell immunofluorescence, the fixed cells were blocked with 5% BSA for 30 min and incubated with GSDMD(N) (1:200 dilution, v/v; Affinity Biosciences LTD., Changzhou, China)/ZO-1 (1:200 dilution, v/v; Proteintech Group, Rosemont, IL, USA) antibodies at 4°C overnight, followed by incubation with FITC-labeled (1:200 dilution, v/v; Beyotime Biotechnology, Shanghai, China)/Cy3-labeled (1:200 dilution, v/v; Beyotime Biotechnology, Shanghai, China) secondary antibodies at RT for 1 h. Cell nuclei were then stained with DAPI (10 μg/mL) at RT for 10 min. For renal double immunofluorescence staining, 5-μm thick frozen sections were blocked with 10% calf serum and incubated with GSDMD(N) (1:200 dilution, v/v)/Synaptopodin (1:500 dilution, v/v; Santa Cruz Biotechnology, Inc., Dallas, TX, USA) and GSDMD(N) (1:200 dilution, v/v)/ZO-1 (1:200 dilution, v/v) at RT overnight and subsequently incubated with FITC-labeled (1:200 dilution, v/v)/Cy3-labeled (1:200 dilution, v/v) secondary antibodies at RT for 40 min. The sections were observed, and photomicrographs were obtained with confocal microscopy.

Immunohistochemistry

After antigen retrieval with Tris-EDTA (pH = 8.0) and blocked with 10% calf serum, sections were incubated with the following antibodies: Desmin (use commercial diluted solution directly; Maixin Biotech, Co., Ltd., Fuzhou, China), WT-1 (1:300 dilution, v/v; Abcam plc, Cambridge, UK), GSDMD(N) (1:200 dilution, v/v), NF-κB p65 (1:500 dilution, v/v; Proteintech Group, Rosemont, IL, USA), p-NF-κB p65 (Ser536) (1:500 dilution, v/v; Affinity Biosciences LTD., Changzhou, China), NLRP3 (1:200 dilution, v/v; Affinity Biosciences LTD., Changzhou, China), ASC (1:200 dilution, v/v; Affinity Biosciences LTD., Changzhou, China), Caspase-1 (1:200 dilution, v/v; Cell Signaling Technology, Inc., Danvers, MA, USA), IL-1β (1:200 dilution, v/v; Cell Signaling Technology, Inc., Danvers, MA, USA) and IL-18 (1:200 dilution, v/v; Affinity Biosciences LTD., Changzhou, China) at RT overnight. Sections were then sequentially incubated with HRP-conjugated secondary antibody (Quanhui Imp & Exp Int'l Co., Ltd., Zhuhai, China) at RT for 40 min and diaminobenzidine chromogen for 15 s to 3 min, counterstained with hematoxylin for 10 min and sealed with neutral balsam. The sections were observed, photomicrographs were acquired with a light microscope, and 3 randomly selected glomeruli from each section were included in semiquantitative analysis with Image-Pro Plus 6.0 software (Media Cybernetics, Rockville, MD, USA). The integrated optical density (IOD) value and the area of each glomerulus were calculated, and the average IOD/area of all 3 glomeruli per section was regarded as the protein expression level of the sample.

RT-qPCR

Glomeruli were isolated from the fresh renal cortex of rats according to Dr. Salant's protocol [15]. Glomerular RNA was extracted using a MiniBEST Universal RNA Extraction Kit (Takara Biomedical Technology Co., Ltd., Shiga, Japan) and reverse transcribed with PrimeScript™ RT Master Mix (Takara Biomedical Technology Co., Ltd., Shiga, Japan) according to the manufacturers' protocols. qPCR was performed according to the protocol of TB Green®Premix Ex Taq™ II (Takara Biomedical Technology Co., Ltd., Shiga, Japan) using the Fast Real-Time PCR System (7900HT, Thermo Fisher Scientific Inc., Waltham, MA, USA). The primers used were as follows: GSDMD (F: 5′'-AGATCGTGGATCATGCCGTC-3′; R: 5′-AGGAGGCAGTAGGGCTTGAA-3′); NLRP3 (F: 5′-CCTTCTGAACCGAGACGTGA-3′; R: 5′-CCAAAGAGGAAGCGTACAACA-3′); ASC (F:5′-GCTGAGCAGCTGCAAAAGAT-3′; R: 5′-GCAATGAGTGCTTGCCTGTG-3′); Caspase-1 (F: 5′-TAGACTACAGATGCCAACCAC-3'; R: 5′-CTTCTTATTGGCATGATTCCC-3′); IL-1β (F: 5′-CAGAAGAATCTAGTTGTCCGT-3′; R: 5′-TGTGCTTCATTCATAAACACT-3′); IL-18 (F: 5′-TATCGACCGAACAGCCAACG-3′; R: 5′-GATAGGGTCACAGCCAGTCC-3′); GAPDH (F: 5′- GCTCTCTGCTCCTCCCTGTTCT-3′; R: 5′-GGCAACAATGTCCACTTTGTCAC-3′). The relative quantity of each gene in every sample was calculated and compared via the $2^{-\Delta\Delta Ct}$ method.

Western Blot

Total protein was extracted from cultured podocytes and rat renal cortex samples with lysis buffer mixed with protease/phosphatase inhibitors (Beyotime Biotechnology, Shanghai, China), while nuclear protein was extracted from rat renal cortex samples with a Nuclear and Cytoplasmic Protein Extraction Kit (KeyGEN Biotech, Nanjing, China). Equal amounts of denatured protein samples from different samples were mixed with loading buffer, separated by SDS–PAGE, and transferred to PVDF membranes. After blocking with 5% BSA, the membranes were separately incubated with the following antibodies: GSDMD (1:1,500 dilution, v/v; Affinity Biosciences LTD., Changzhou, China), NF-kB p65 (1:1,000 dilution, v/v), p-NF-kB p65 (Ser536) (1:1,000 dilution, v/v), NLRP3 (1:1,000 dilution, v/v), ASC (1:1,000 dilution, v/v), Caspase-1 (1:1,000 dilution, v/v), IL-1β (1:1,000 dilution, v/v), IL-18 (1:1,000 dilution, v/v), GAPDH (1:3,000 dilution, v/v; Cwbio IT Group, Beijing, China) and Histone H3 (1:3,000 dilution, v/v; Proteintech Group, Rosemont, IL, USA) at 4°C overnight. After incubation with an HRP-conjugated secondary antibody (1:5,000 dilution, v/v; TransGen Biotech, Beijing, China) at RT for 2 h, the protein bands were visualized using Immobilon™ Western Chemiluminescent HRP Substrate (Merck KGaA, Darmstadt, Germany) and photographed using an automatic chemiluminescence/fluorescence image analysis system (5200, Tanon Science & Technology Co., Ltd., Shanghai, China).

ELISA

IL-18 release in the culture supernatant of the podocytes and the serum IL-1β/IL-18 levels of rats were tested using human IL-18 ELISA and rat IL-1β/IL-18 ELISA kits (Boster Biological Technology Co. Ltd., Wuhan, China), respectively. Samples were prepared and measured strictly in accordance with the manufacturers' protocols.

Statistics

All experiments were carried out at least three times. Statistical analyses were performed with SPSS 20.0 software (IBM Corporation, Armonk, NY, USA). Data are shown as the mean ± standard deviation (SD). ANOVA with LSD-t test (equal variances assumed) or the Welch test with Dunnett's T3 test (equal variances not assumed) was used for multiple comparisons among groups. All tests were two-sided, and $p < 0.05$ was considered indicative of statistical significance.

Results

DSF Alleviated C3a/C5a-Induced Podocyte Injury by Inhibiting Pyroptosis

Given that DSF can inhibit pyroptosis by preventing GSDMD pore formation, we first examined the inhibitory effect of DSF on complement-induced podocyte pyroptosis. As shown in Figure 1a, cell immunofluorescence staining showed that signs of activation and membrane translocation of GSDMD, manifested by the colocalization of activated N-terminal fragment of GSDMD (GSDMD(N)) and cytomembrane marker ZO-1 in C3a/C5a-treated podocytes, were significantly suppressed by DSF. Moreover, DSF reduced the increase and activation of the pyroptosis signaling pathway NLRP3-ASC-Caspase-1-IL-18/GSDMD in C3a/C5a-treated podocytes (Fig. 1b). Meanwhile, the increase and activation of one of the key upstream stimulators of NLRP3, NF-κB, were also inhibited by DSF (Fig. 1b). The increased release of the pyroptosis-associated cytokine IL-18, probably derived from the activation of the pyroptosis signaling pathway in C3a/C5a-treated podocytes, was also reduced after DSF treatment (Fig. 1c). On this basis, we further examined the effect of DSF on podocyte injury and found that injury to C3a/C5a-treated podocytes, reflected by the increased percentage of PI staining cells and increased release of LDH, was significantly alleviated by DSF (Fig. 1d, e and f). Taken together, the in vitro experiments validated the protective effect of DSF on C3a/C5a-induced podocyte injury by inhibiting pyroptosis.

DSF Ameliorated Renal Lesions and Podocyte Injury in PHN Rats

On the basis of the in vitro experiments, we continued to explore the effects of DSF on renal lesions and podocyte injury in PHN rats. The rats were randomly divided into 3 groups: NC, PHN and PHN + DSF ($n = 6$/group). During the 15-day observation period, the rats in different groups showed similar growth trends (Fig. 2a). This result suggested, to some extent, the rats tolerated the current dosage of DSF well. Compared to those in the NC group, rats in the PHN group showed typical nephrotic syndrome with a significant increase in 24 h-UPro and a decrease in ALB after model establishment, while those in the PHN + DSF group showed significant amelioration (Fig. 2b, c). The levels of SCr were elevated in the PHN group and decreased in the DSF treatment group (Fig. 2d). BUN, an indicator of glomerular filtration function, remained largely unchanged in each group of rats throughout the observation period (Fig. 2e). Hyperlipemia, another typical manifestation of nephrotic syndrome that includes increased T-CHOL, TG, HDL and LDL, was also observed after PHN model establishment. Compared with the NC group, the PHN and PHN + DSF groups exhibited gradual increases in the levels of T-CHOL, HDL and LDL during the course of the experiment, and there were no significant differences between the PHN and PHN + DSF groups (Fig. 2f, h and i). However, DSF significantly reduced the increased level of TG in the PHN group on day 15 during the observation period (Fig. 2g). Taken together, these results indicated that DSF could alleviate renal lesions in PHN rats.

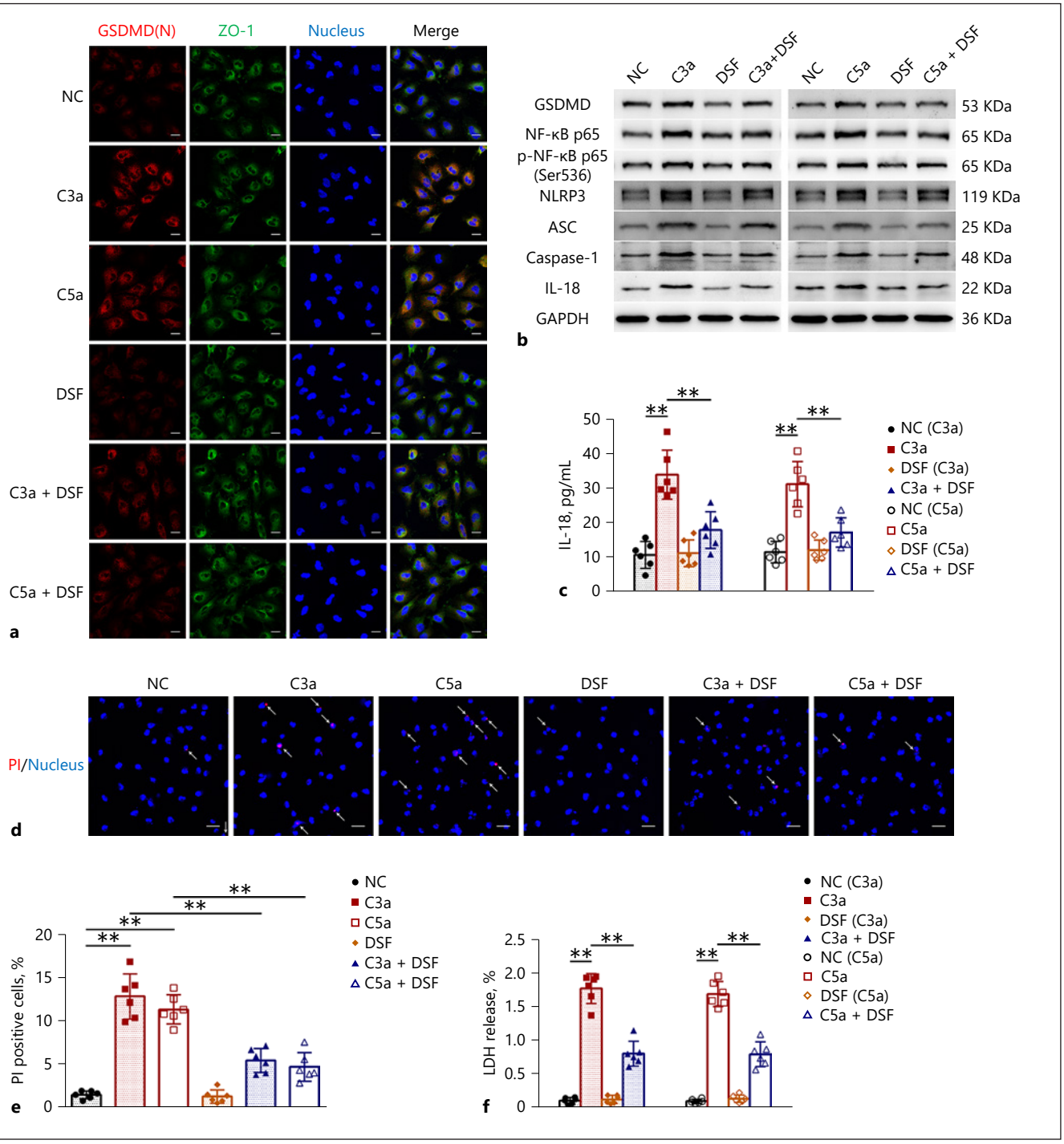

Fig. 1. DSF alleviated C3a/C5a-induced podocyte injury by inhibiting pyroptosis. Podocyte injury was induced with C3a (50 nM) and C5a (50 nM). The inhibitory effects of DSF (250 nM) on C3a/C5a-induced pyroptosis were examined. **a** Representative images of GSDMD(N)/ZO-1/Nucleus (DAPI) triple immunofluorescent staining of treated podocytes. Scale bars = 20 μm. **b** Representative Western Blot images of GSDMD, NF-κB p65, p-NF-κB p65 (Ser536), NLRP3, ASC, Caspase-1, IL-18 and the internal control (GAPDH) in treated podocytes. **c** IL-18 release in treated podocytes was detected. **d**, **e** Representative images of PI/Nucleus (DAPI) double fluorescent staining of treated podocytes (**d**) and percentage of PI-positive cells (**e**); arrows, PI-positive cells; scale bars = 40 μm. **f** LDH release in treated podocytes was detected. The data above represent three independent experiments in duplicate and are shown as the mean ± SD, and ANOVA with LSD-t test (equal variances assumed) or Welch's test with Dunnett's T3 test (equal variances not assumed) was used for multiple comparisons among groups. *, $p < 0.05$; **, $p < 0.01$.

Kidney Dis 2022;8:308–318
DOI: 10.1159/000524164

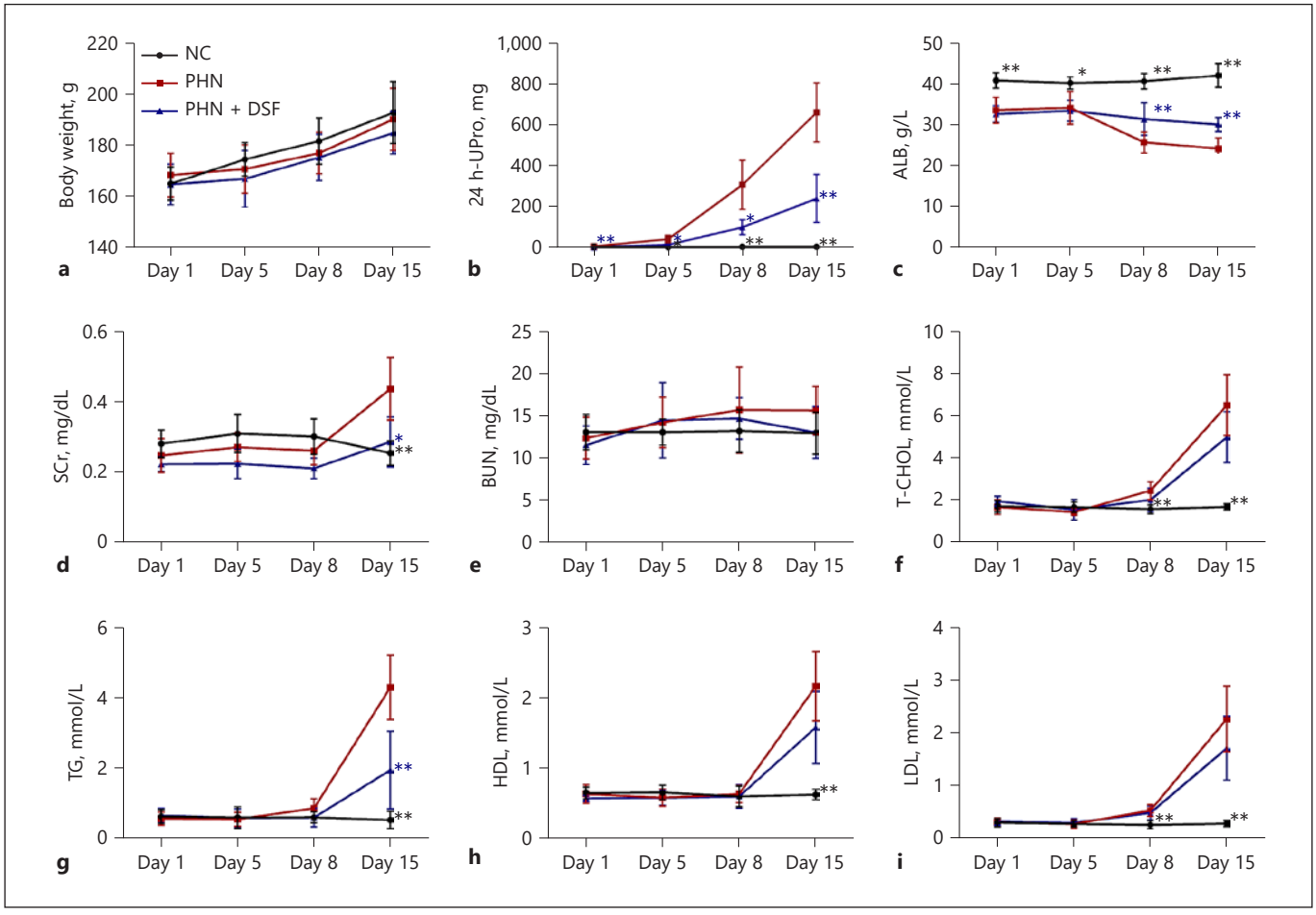

Fig. 2. DSF alleviated the renal lesions in PHN rats. Body weight (**a**), 24 h-UPro (**b**), ALB (**c**), SCr (**d**), BUN (**e**), T-CHOL (**f**), TG (**g**), HDL (**h**), and LDL (**i**) of rats ($n = 6$) in each group were evaluated on days 1, 5, 8, and 15 after model establishment. The data above are shown as the mean ± SD and were compared to the PHN group. ANOVA with LSD-t test (equal variances assumed) or Welch's test with Dunnett's T3 test (equal variances not assumed) was used for multiple comparisons among groups. *, $p < 0.05$; **, $p < 0.01$.

We further validated the effect of DSF on podocyte injury in PHN rats. Masson and PASM-Masson staining of the renal tissue in PHN rats revealed pathological features of MN, including subepithelial deposits of fuchsin protein and spike-like changes in the GBM (Fig. 3a). Desmin, one of the most common markers of podocyte injury, increased significantly in the glomeruli of PHN rats while WT-1, another indicator of podocyte injury, manifested decreased expression in the nuclei of podocyte and abnormal distribution in the glomeruli of PHN rats (Fig. 3b, c). Under transmission electron microscopy, characteristic manifestations of MN, including subepithelial dense deposits and widespread foot process fusion of podocytes, delineated by a significant increase in foot process width, were observed in the glomeruli of PHN rats (Fig. 3d, e). Compared to PHN rats, the increased expression of glomerular Desmin, the decreased podocytes nuclear expression and abnormal glomerular distribution of WT-1, as well as foot process fusion of podocytes were all notably alleviated after DSF treatment (Fig. 3b, c, d and e), suggesting the protective effect of DSF on podocyte injury in MN. We also evaluated the effect of DSF on immune complex deposition and complement system activation in the glomeruli of PHN rats; however, no significant difference was found between the PHN and PHN + DSF groups (data not shown).

DSF Inhibited Podocyte Pyroptosis in PHN Rats

We proceeded to explore whether the protective effect of DSF on PHN rats could be attributed to its anti-pyrop-

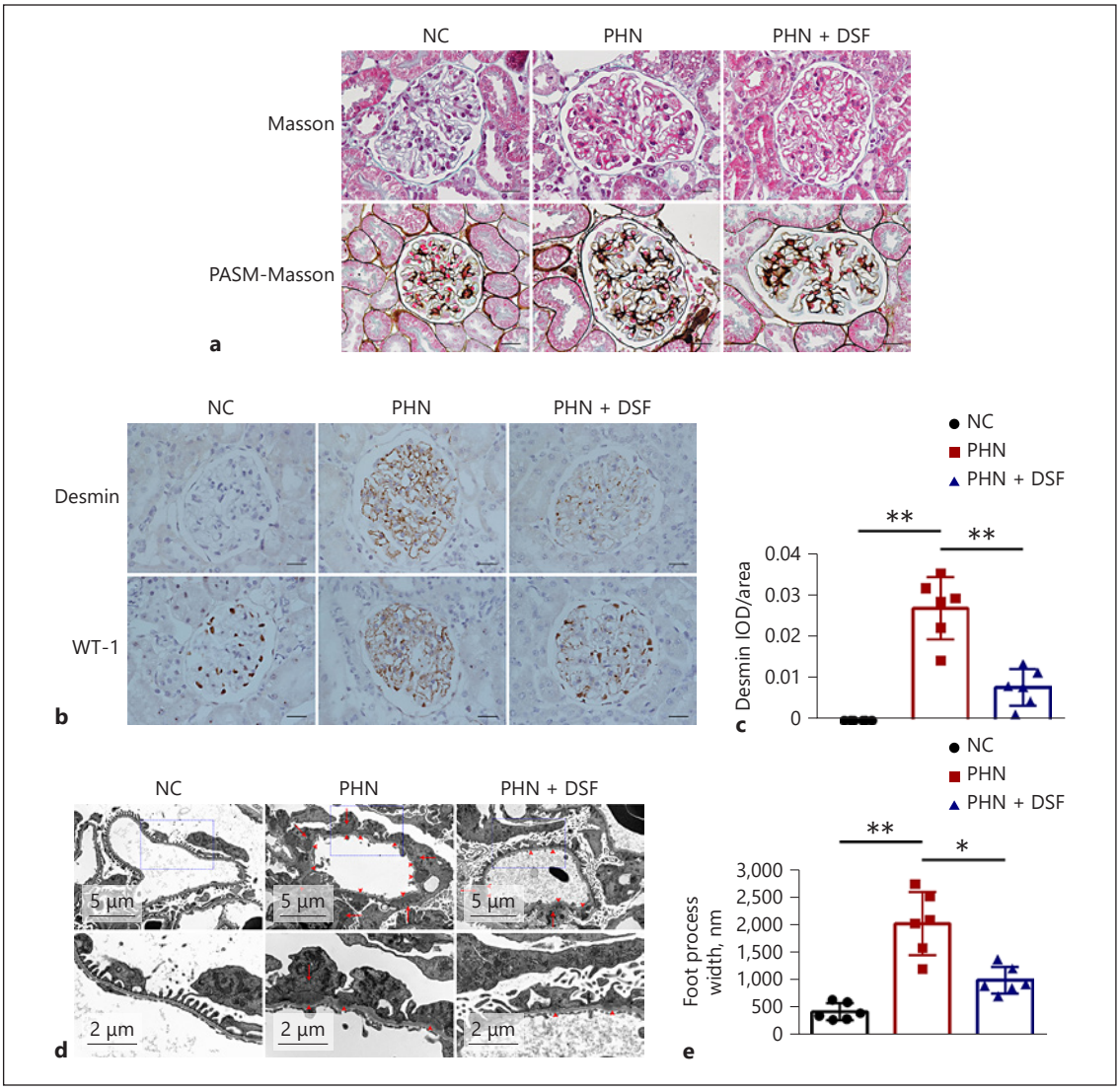

Fig. 3. DSF ameliorated glomerular podocyte injury in PHN rats. **a** Representative renal Masson and PASM-Masson staining of the rats ($n = 6$) in each group; Scale bars = 20 μm. **b**, **c** Representative renal immunohistochemical staining of Desmin and WT-1 (**b**) and semiquantification based on the glomerular IOD/area of Desmin (**c**) of the rats ($n = 6$) in each group; Scale bars = 20 μm. **d**, **e** Representative glomerular transmission electron microscopy images (**d**) and podocyte foot process width (**e**) of the rats ($n = 6$) in each group. Arrowheads, subepithelial dense deposit; arrows, podocyte foot process fusion. The data above are shown as the mean ± SD. ANOVA with LSD-t test (equal variances assumed) or Welch's test with Dunnett's T3 test (equal variances not assumed) was used for multiple comparisons among groups. *, $p < 0.05$; **, $p < 0.01$.

Fig. 4. DSF inhibited the renal pyroptosis signaling pathway in PHN rats. **a** Representative renal GSDMD(N)/Synaptopodin and GSDMD(N)/ZO-1 double immunofluorescent staining of the rats ($n = 6$) in each group; Scale bars = 20 μm. **b**, **c** Representative renal immunohistochemical staining (**b**) and semiquantification based on the glomerular IOD/area of GSDMD(N), NF-κB p65, p-NF-κB p65 (Ser536), NLRP3, ASC, Caspase-1, IL-1β, and IL-18 (**c**) of the rats ($n = 6$) in each group; Scale bars = 20 μm. **d** Relative mRNA levels of glomerular GSDMD, NLRP3, ASC, Caspase-1, IL-1β and IL-18 of the rats ($n = 6$) in each group. **e** Representative Western Blot images of renal GSDMD, NF-κB p65, p-NF-κB p65 (Ser536), nuclear NF-κB p65, nuclear p-NF-κB p65 (Ser536), NLRP3, ASC, Caspase-1, Caspase-1 p20, IL-1β, IL-1β (mature form), IL-18 and the internal control (GAPDH, Histone H3) of the rats ($n = 6$) in each group. Serum IL-1β (**f**) and IL-18 (**g**) of the rats ($n = 6$) in each group on days 1, 5, 8, 15 after model establishment. The data above are shown as the mean ± SD (**c**, **d**, **f**, **g**) and were compared to the PHN group (**f**, **g**). ANOVA with LSD-t test (equal variances assumed) or Welch's test with Dunnett's T3 test (equal variances not assumed) was used for multiple comparisons among groups. *, $p < 0.05$; **, $p < 0.01$.

(For figure see next page.)

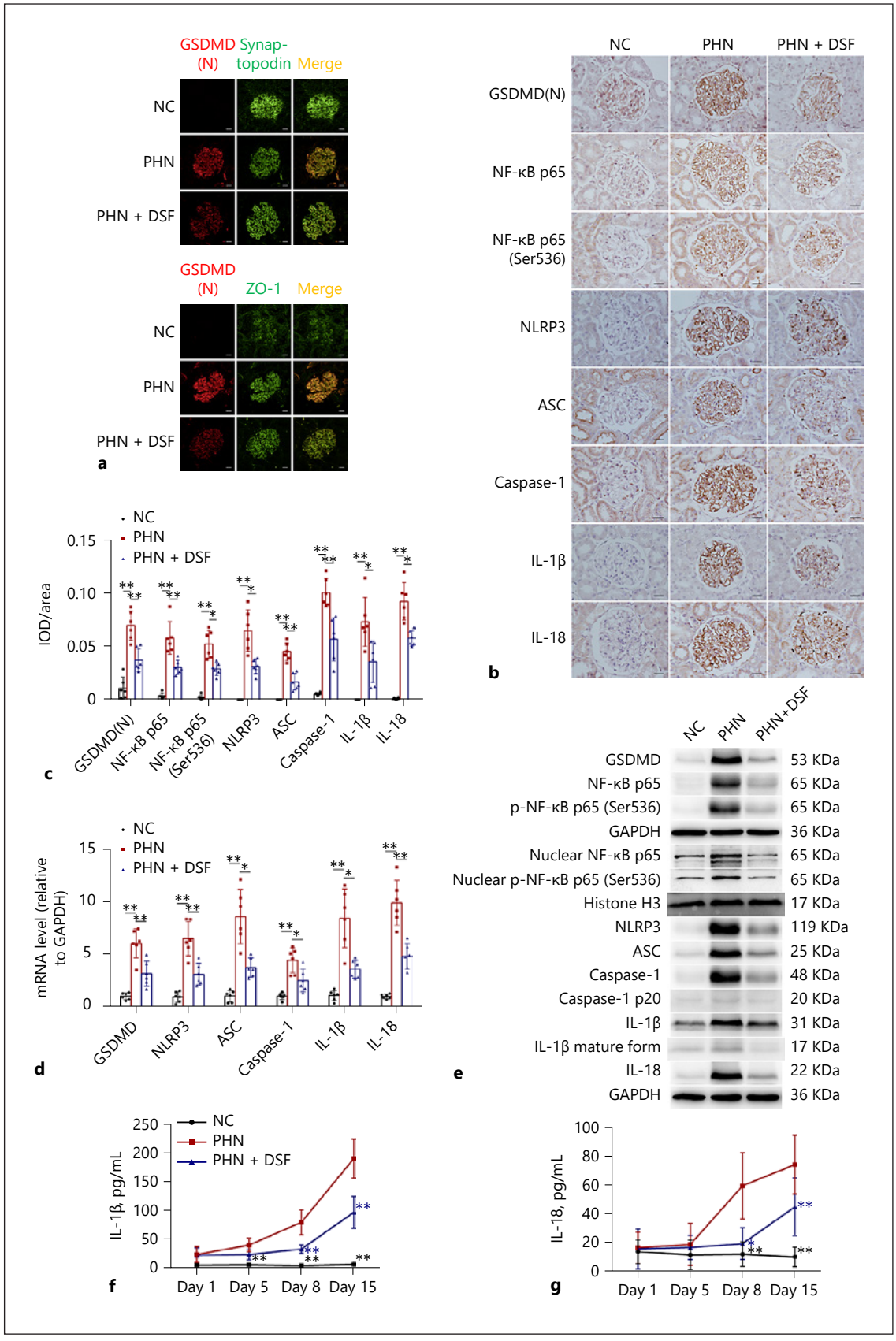
GSDMD (N)
Synap-topodin
Merge
NC
PHN
PHN + DSF
GSDMD (N)
ZO-1
Merge
NC
PHN
PHN + DSF
a
NC
PHN
PHN + DSF
GSDMD(N)
NF-κB p65
NF-κB p65 (Ser536)
NLRP3
ASC
Caspase-1
IL-1β
IL-18
b
NC
PHN
PHN + DSF
IOD/area
0.15
0.10
0.05
0
GSDMD(N)
NF-κB p65
NF-κB p65 (Ser536)
NLRP3
ASC
Caspase-1
IL-1β
IL-18
c
NC
PHN
PHN + DSF
mRNA level (relative to GAPDH)
15
10
5
0
GSDMD
NLRP3
ASC
Caspase-1
IL-1β
IL-18
d
NC
PHN
PHN+DSF
GSDMD 53 KDa
NF-κB p65 65 KDa
p-NF-κB p65 (Ser536) 65 KDa
GAPDH 36 KDa
Nuclear NF-κB p65 65 KDa
Nuclear p-NF-κB p65 (Ser536) 65 KDa
Histone H3 17 KDa
NLRP3 119 KDa
ASC 25 KDa
Caspase-1 48 KDa
Caspase-1 p20 20 KDa
IL-1β 31 KDa
IL-1β mature form 17 KDa
IL-18 22 KDa
GAPDH 36 KDa
e
NC
PHN
PHN + DSF
IL-1β, pg/mL
250
200
150
100
50
0
Day 1
Day 5
Day 8
Day 15
f
IL-18, pg/mL
100
80
60
40
20
0
Day 1
Day 5
Day 8
Day 15
g

4

tosis effect. Similar to our findings in vitro, the double immunofluorescence test clearly depicted the translocation process of activated GSDMD to the membrane of podocytes, namely, the occurrence of pyroptosis in podocytes, reflected by the increased colocalization of GSDMD(N) with the podocyte marker Synaptopodin and the cytomembrane marker ZO-1 (Fig. 4a). This phenomenon was significantly inhibited following DSF administration (Fig. 4a). In addition, the increase and activation of the NLRP3-ASC-Caspase-1/IL-1β/IL-18/GSDMD pyroptosis signaling pathway in the glomeruli of PHN rats, reflected by the glomerular increased expression of GSDMD, NLRP3, ASC, Caspase-1, IL-1β, and IL-18 at the protein (Fig. 4b, c, e) and mRNA (Fig. 4d) levels, were all significantly inhibited after DSF treatment (Fig. 4b, c, d and e). The increase in the activating forms of Caspase-1 (Caspase-1 p20) and IL-1β (IL-1β mature form) in renal tissues (Fig. 4e) was also inhibited by DSF. Furthermore, the increased levels of circulating IL-1β and IL-18 in PHN rats also declined after DSF treatment (Fig. 4f, g). We also extended our observation to alterations in the NF-κB signaling pathway within the kidneys of PHN rats. Similar to our in vitro findings, the increase and activation of NF-κB p65 and p-NF-κB p65 (Ser536) reappeared in the glomeruli of PHN rats (Fig. 4b, c and e). DSF manifested similar inhibitory effects on the increase and activation of the NF-κB signaling pathway (Fig. 4b, c and e). The parallel increase and activation of the NF-κB and pyroptosis signaling pathways in vitro and in vivo preliminarily suggested a regulatory effect of NF-κB on pyroptosis of podocytes in MN. To summarize, based on these findings, we can conclude that the protective effect of DSF on renal lesions and podocyte injury in PHN rats, at least in part, can be ascribed to its anti-pyroptosis effect.

Discussion

Treatment of MN remains to be explored at present. Although clinical remission rates are improving greatly due to the application of cyclophosphamide, calcineurin inhibitors, and especially CD20-targeted agents, the efficacy of these drugs in preventing MN progression remains to be validated [1, 17]. Therefore, exploring more effective targeted drugs for renal injury in MN is crucial to improve the long-term outcome of patients. As a lytic and highly inflammatory regulated cell death program, pyroptosis occurs downstream of inflammasome activation and is driven by members of the gasdermin family, most notably GSDMD. Recently, a body of evidence has suggested the involvement of pyroptosis in kidney diseases. In a murine model of acute kidney injury (AKI), proteins in the pyroptosis signaling pathway, including Caspase-1, Caspase-11, IL-1β, and GSDMD, were significantly increased, accompanied by elevated renal structural and functional injury [18, 19]. GSDMD also increased and was activated in the kidneys of db/db mice and diabetic nephropathy (DN) patients with the development of tubular injury, demonstrating the close relationship between pyroptosis and DN [20]. Pyroptosis was also associated with lupus nephritis (LN) since an increase and activation of GSDMD can be detected in the kidneys of LN patients and mice [21]. Our previous work also depicted the pivotal role of pyroptosis in mediating podocyte injury in MN [11]. On the other hand, the renal protective effect of inhibitors that target members of the pyroptosis signaling pathway, including NLRP3 and Caspase-1, was also depicted in a murine model of AKI, crystal nephropathy, and unilateral ureter obstruction [22–24]. However, to the best of our knowledge, none of the pyroptosis inhibitors used in renal experiments have been applied in clinical practice. A very long journal still exists from bench to bedside. Therefore, in the current study, we validated the therapeutic effect of an FDA-approved drug, DSF, in the treatment of MN through the inhibition of podocyte pyroptosis in vitro and in vivo.

DSF is an inexpensive, accessible and safe drug and has been commonly used for alcohol addiction in clinical practice since the 1950s. It is an inhibitor of aldehyde dehydrogenase that is responsible for the conversion of alcohol into acetaldehyde [12]. DSF was also found to have an antitumor effect on several types of cancer, including non-small-cell lung cancer, liver cancer, breast cancer, prostate cancer, pancreatic cancer, glioblastoma and melanoma, by inhibiting the NF-κB signaling pathway, proteasome activity, and aldehyde dehydrogenase activity and inducing endoplasmic reticulum stress and autophagy [25]. The excellent safety of DSF also remained in some clinical trials that evaluated its effect against cancer [25]. Recently, Hu et al. [13] found that DSF could block pore formation by GSDMD by covalently modifying Cys191/Cys192 of human/mouse GSDMD and therefore had an anti-pyroptotic effect. Our study reconfirmed the anti-pyroptotic effect of DSF in podocytes since a similar inhibi-

tory effect on GSDMD pore formation in podocytes of human and PHN rats, manifested by decreased cytomembrane transfer of GSDMD(N), can also be observed in human podocytes treated with C3a/C5a and podocytes in PHN rats. The protective effect of DSF was evident since significant relief of podocyte injury caused by C3a/C5a in vitro and alleviation of nephrotic syndrome, abnormal alterations of podocyte injury markers and podocyte foot process fusion in vivo were observed after DSF treatment.

Interestingly, in our experiment, DSF showed an additional inhibitory effect on the NF-κB and pyroptosis signaling pathways rather than merely inhibiting GSDMD within the podocyte and kidney. This phenomenon was also observed in Hu et al.'s [26] work, where DSF inhibited the activation of NF-κB, NLRP3, ASC, Caspase-1 and IL-1β in vitro as well. In another study in which a mouse model of AKI was investigated, DSF also manifested a similar inhibitory effect on the expression of NLRP3, cleaved Caspase-1 and IL-1β in the kidneys [27]. The "multiple" effect of DSF in our study may be first explained by its anti-inflammatory and antioxidative effects. In a rat model of cisplatin-induced acute nephrotoxicity, DSF can dampen the increase in pro-inflammatory cytokines, including TNF-α and IL-1β, and reverse the depletion of antioxidases, including SOD, catalase and GSH, within the kidney [28]. The anti-inflammatory and antioxidative effects of DSF were also observed in extrarenal organs such as the liver and eye [29–32]. It is known that the activation of canonical inflammasomes includes two steps, priming and activation, and both steps are influenced by inflammation and oxidative stress [10]. As a consequence, downregulation of NF-κB and the whole pyroptosis signaling pathway in our observation may partially reflect the anti-inflammatory and antioxidative effects of DSF. Second, the inflammatory milieu caused by the maturation and release of IL-1β and IL-18 during the pyroptosis process also helped to promote the activation of NF-κB and NLRP3 [10]; therefore, the decreased release of IL-1β and IL-18 due to GSDMD pore inhibition by DSF may in turn alleviate the pyroptosis process, namely, the disruption of the vicious cycle of pyroptosis may also be attributable to the "multiple" effect of DSF. Finally, DSF had a direct inhibitory effect on NF-κB. Preliminary data from Kanai et al. [29, 30] revealed the inhibitory effect of NF-κB after topical and systemic administration of DSF in rats with endotoxin-induced uveitis. The inhibitory effect of DSF on NF-κB was also depicted in several tumor cell lines, including lymphoid malignant cells, breast cancer stem cells and hepatocellular carcinoma cells [33–36]. In summary, the overall inhibition of the pyroptosis signaling pathway rather than simply the inhibition of GSDMD pore formation may probably be responsible for the protective effect of DSF in MN.

Conclusion

The FDA-approved drug DSF can alleviate MN by inhibiting podocyte pyroptosis. The findings highlighted the potential role of DSF in the treatment of MN patients in the future.

Statement of Ethics

This study protocol of animals was reviewed and approved by the Institutional Animal Care and Use Committee (IACUC) of Jinling Hospital, the First School of Clinical Medicine of Southern Medical University, Nanjing, China (Approval reference number: 2019JLHGKJDWLS-136).

Conflict of Interest Statement

The authors have no conflicts of interest to declare.

Funding Sources

This work was supported by grants from the National Natural Science Foundation of China Special Project (No. 32141004) and the National Key Technology R&D Program of China (No. 2015BAI12B02).

Author Contributions

D. Lv performed the experiments, collected and analyzed the data, and wrote the manuscript; S. Jiang, M. Zhang, X. Zhu, F. Yang, H. Wang, S. Li, F. Liu, C. Zeng and W. Qin performed the experiments, collected and analyzed the data; L. Li and Z. Liu conceived the study and revised the manuscript. All authors reviewed and approved the manuscript.

Data Availability Statement

All data generated or analyzed during this study are included in this article. Further inquiries can be directed to the corresponding author.

References

1 Couser WG. Primary membranous nephropathy. Clin J Am Soc Nephrol. 2017 Jun 7;12(6):983–97.
2 Narasimhan B, Chacko B, John GT, Korula A, Kirubakaran MG, Jacob CK. Characterization of kidney lesions in Indian adults: towards a renal biopsy registry. J Nephrol. 2006 Mar-Apr;19(2):205–10.
3 Polito MG, de Moura LA, Kirsztajn GM. An overview on frequency of renal biopsy diagnosis in Brazil: clinical and pathological patterns based on 9,617 native kidney biopsies. Nephrol Dial Transplant. 2010 Feb;25(2):490–6.
4 Hou JH, Zhu HX, Zhou ML, Le WB, Zeng CH, Liang SS, et al. Changes in the spectrum of kidney diseases: an analysis of 40,759 biopsy-proven cases from 2003 to 2014 in China. Kidney Dis. 2018 Feb;4(1):10–9.
5 Debiec H, Lefeu F, Kemper MJ, Niaudet P, Deschênes G, Remuzzi G, et al. Early-childhood membranous nephropathy due to cationic bovine serum albumin. N Engl J Med. 2011 Jun 2;364(22):2101–10.
6 Takano T, Elimam H, Cybulsky AV. Complement-mediated cellular injury. Semin Nephrol. 2013 Nov;33(6):586–601.
7 Sethi S. New "antigens" in membranous nephropathy. J Am Soc Nephrol. 2021 Feb;32(2):268–78.
8 Broz P, Pelegrín P, Shao F. The gasdermins, a protein family executing cell death and inflammation. Nat Rev Immunol. 2020 Mar;20(3):143–57.
9 He WT, Wan H, Hu L, Chen P, Wang X, Huang Z, et al. Gasdermin D is an executor of pyroptosis and required for interleukin-1β secretion. Cell research. 2015 Dec;25(12):1285–98.
10 Komada T, Muruve DA. The role of inflammasomes in kidney disease. Nat Rev Nephrol. 2019 Aug;15(8):501–20.
11 Wang Hui, Lv Daoyuan, Jiang Song, Hou Qing, Zhang Lei, Li Shen, et al. Complement induces podocyte pyroptosis in membranous nephropathy by mediating mitochondrial dysfunction. Cell Death Dis. 2022;13(3):281.
12 Dalecki AG, Crawford CL, Wolschendorf F. Copper and antibiotics: discovery, modes of action, and opportunities for medicinal applications. Adv Microb Physiol. 2017;70:193–260.
13 Hu JJ, Liu X, Xia S, Zhang Z, Zhang Y, Zhao J, et al. FDA-approved disulfiram inhibits pyroptosis by blocking gasdermin D pore formation. Nat Immunol. 2020 Jul;21(7):736–45.
14 Saleem MA, O'Hare MJ, Reiser J, Coward RJ, Inward CD, Farren T, et al. A conditionally immortalized human podocyte cell line demonstrating nephrin and podocin expression. J Am Soc Nephrol. 2002 Mar;13(3):630–8.
15 Salant DJ, Cybulsky AV. Experimental glomerulonephritis. Methods Enzymol. 1988;162:421–61.
16 White KE, Bilous RW. Estimation of podocyte number: a comparison of methods. Kidney Int. 2004;66(2):663–7.
17 Cattran DC, Brenchley PE. Membranous nephropathy: integrating basic science into improved clinical management. Kidney Int. 2017 Mar;91(3):566–74.
18 Yang JR, Yao FH, Zhang JG, Ji ZY, Li KL, Zhan J, et al. Ischemia-reperfusion induces renal tubule pyroptosis via the CHOP-caspase-11 pathway. Am J Physiol Renal Physiol. 2014 Jan 1;306(1):F75–84.
19 Li Y, Xia W, Wu M, Yin J, Wang Q, Li S, et al. Activation of GSDMD contributes to acute kidney injury induced by cisplatin. Am J Physiol Renal Physiol. 2020 Jan 1;318(1):F96–106.
20 Wang Y, Zhu X, Yuan S, Wen S, Liu X, Wang C, et al. TLR4/NF-κB signaling induces GSDMD-related pyroptosis in tubular cells in diabetic kidney disease. Front Endocrinol. 2019;10:603.
21 Cao H, Liang J, Liu J, He Y, Ke Y, Sun Y, et al. Novel effects of combination therapy through inhibition of caspase-1/gasdermin D induced-pyroptosis in lupus nephritis. Front Immunol. 2021;12:720877.
22 Cao Y, Fei D, Chen M, Sun M, Xu J, Kang K, et al. Role of the nucleotide-binding domain-like receptor protein 3 inflammasome in acute kidney injury. FEBS J. 2015 Oct;282(19):3799–807.
23 Ludwig-Portugall I, Bartok E, Dhana E, Evers BD, Primiano MJ, Hall JP, et al. An NLRP3-specific inflammasome inhibitor attenuates crystal-induced kidney fibrosis in mice. Kidney Int. 2016 Sep;90(3):525–39.
24 Sogawa Y, Nagasu H, Iwase S, Ihoriya C, Itano S, Uchida A, et al. Infiltration of M1, but not M2, macrophages is impaired after unilateral ureter obstruction in Nrf2-deficient mice. Sci Rep. 2017 Aug 18;7(1):8801.
25 Lu C, Li X, Ren Y, Zhang X. Disulfiram: a novel repurposed drug for cancer therapy. Cancer Chemother Pharmacol. 2021 Feb;87(2):159–72.
26 Hu JJ, Liu X, Zhao J, Xia S, Ruan J, Luo X, et al. Identification of pyroptosis inhibitors that target a reactive cysteine in gasdermin D. bioRxiv; 2018:365908.
27 Huang J, Wei S, Peng Z, Xiao Z, Yang Y, Liu J, et al. Disulfiram attenuates lipopolysaccharide-induced acute kidney injury by suppressing oxidative stress and NLRP3 inflammasome activation in mice. J Pharm Pharmacol. 2021 Dec 19;74(2):259–67.
28 Khairnar SI, Mahajan UB, Patil KR, Patel HM, Shinde SD, Goyal SN, et al. Disulfiram and its copper chelate attenuate cisplatin-induced acute nephrotoxicity in rats via reduction of oxidative stress and inflammation. Biol Trace Elem Res. 2020 Jan;193(1):174–84.
29 Kanai K, Itoh N, Yoshioka K, Yonezawa T, Ikadai H, Hori Y, et al. Inhibitory effects of oral disulfiram on endotoxin-induced uveitis in rats. Curr Eye Res. 2010 Oct;35(10):892–9.
30 Kanai K, Ito Y, Nagai N, Itoh N, Hori Y, Chikazawa S, et al. Effects of instillation of eyedrops containing disulfiram and hydroxypropyl-β-cyclodextrin inclusion complex on endotoxin-induced uveitis in rats. Curr Eye Res. 2012 Feb;37(2):124–31.
31 Schwartz JJ, Emerson L, Hillas E, Phan A, Thiesset H, Firpo M, et al. Amelioration of hepatic inflammation in a mouse model of NASH using a dithiocarbamate derivative. Hepatol Int. 2013 Jun;7(2):600–9.
32 Begic A, Djuric A, Ninkovic M, Stevanovic I, Djurdjevic D, Pavlovic M, et al. Disulfiram moderately restores impaired hepatic redox status of rats subchronically exposed to cadmium. J Enzyme Inhib Med Chem. 2017 Dec;32(1):478–89.
33 Liu P, Wang Z, Brown S, Kannappan V, Tawari PE, Jiang W, et al. Liposome encapsulated disulfiram inhibits NFκB pathway and targets breast cancer stem cells in vitro and in vivo. Oncotarget. 2014 Sep 15;5(17):7471–85.
34 Wang Y, Li W, Patel SS, Cong J, Zhang N, Sabbatino F, et al. Blocking the formation of radiation-induced breast cancer stem cells. Oncotarget. 2014 Jun 15;5(11):3743–55.
35 Zha J, Chen F, Dong H, Shi P, Yao Y, Zhang Y, et al. Disulfiram targeting lymphoid malignant cell lines via ROS-JNK activation as well as Nrf2 and NF-kB pathway inhibition. J Transl Med. 2014 Jun 11;12:163.
36 Li Y, Wang LH, Zhang HT, Wang YT, Liu S, Zhou WL, et al. Disulfiram combined with copper inhibits metastasis and epithelial-mesenchymal transition in hepatocellular carcinoma through the NF-κB and TGF-β pathways. J Cell Mol Med. 2018 Jan;22(1):439–51.